




# Molybdenum oxide reinforced polyvinyl alcohol composite as high-performance dielectric material for flexible electronics

Kiruthika Parangusan<sup>1</sup>, Venkat Subramaniam<sup>1</sup>, Anandha babu Ganesan<sup>2</sup>, P. Sundara Venkatesh<sup>3</sup>, and Deepalekshmi Ponnamma<sup>4,\*</sup> 

<sup>1</sup>Department of Electronics, PSG College of Arts and Science, Coimbatore, Tamilnadu, India

<sup>2</sup>Department of Physics, Bannari Amman Institute of Technology, Sathyamangalam, Tamilnadu, India

<sup>3</sup>Department of Physics, Nanomaterials Laboratory, Sri. S. Ramasamy Naidu Memorial College, Sattur, Tamilnadu 626203, India

<sup>4</sup>Materials Science and Technology Program, Department of Mathematics, Statistics and Physics, College of Arts and Sciences, Qatar University, Doha 2713, Qatar

**Received:** 5 February 2023

**Accepted:** 16 April 2023

**Published online:**

8 May 2023

© The Author(s) 2023

## ABSTRACT

Polymer dielectrics are highlighted as capable energy storing materials due to their better dielectric strength and supreme versatility compared to inorganic ceramic dielectrics in sophisticated electronics and pulsed power systems. The capacity of pristine polymers to store energy, on the other hand, has hardly been constrained by relatively poor internal dielectric properties. This study demonstrates a viable solution-casting method for creating a MoO<sub>3</sub> (0%, 1%, 3%, and 5%) doped PVA-based composites for notable dielectric characteristics. The structural variations and morphological properties in the presence of MoO<sub>3</sub> nanoparticles within the polymer, connected through intra/intermolecular hydrogen bonding are investigated using XRD and FTIR. The influence of MoO<sub>3</sub> content on the complex dielectric properties, conductivities, electric modulus, and impedance parameters of PVA is further investigated. According to the MoO<sub>3</sub> proportion in the host matrix, the dielectric properties and relaxation factors associated with polymer cooperative chain segmental migration alter considerably. The improved electrical and dielectric properties of MoO<sub>3</sub> doped PVA composite demonstrate its potential in creating compact polymer electrolyte systems.

Address correspondence to E-mail: lekshmi\_deepa@yahoo.com

## 1 Introduction

Modern electronics heighten the demand for adaptable, multipurpose, eco-friendly dielectric materials with superior properties. Historically, ceramics were used as dielectric materials; however, it possessed undesirable properties such as brittleness, processing difficulties, and low stability. Polymers have superior flexibility, processability, and light weight when compared to ceramics [1–3]. And they gained significant interest in science and technology during the last decade as a dielectric or interfacial layer between metals and semiconductors [4]. Among the polymers biodegradable, non-toxic, and hydrophilic ones have specific research interest, as they can be applicable in bio electronics. When such polymer films are made using the solution casting method, they provide better flexibility with improved characteristics [5].

Polyvinyl alcohol (PVA) is widely reported for the preparation of polymer composites because of its good mechanical, chemical and thermal stability, excellent flexibility, and high tensile strength. PVA has a very high dielectric strength and an excellent charge storage capacity, making it widely applicable in various industries [6]. It also has a backbone composed of carbon chains, but rather than methane's carbon, it possesses hydroxyl groups. These OH groups act as hydrogen bonding sources and thus aid in the production of functionalized composites [7]. Such resilient intra- and intermolecular hydrogen bonds devised by the hydroxyl (–OH) groups result in a variety of useful physicochemical properties, besides superior chemical resistance, exquisite wettability, thermal properties, stretchability, dielectric strength, as well as charge storage capabilities [5]. The high density of hydroxyl groups, also allows cross-linking via irradiation, chemical, or heat treatment. However, water absorption in PVA is one of the most critical elements influencing its characteristics and applications, though the hydrophilicity favors production of composite films. Ion mobility, ion detachment, and increased polymer mechanical strength were noticed by the addition of nano-ceramic due to the significant interfacial interaction around nanoparticles and PVA [8]. The addition of an appropriate filler can customize the electrical characteristics of PVA to a specific requirement. In general, the chemical composition of the filler, distribution in a given polymer and its interaction with the host matrix influence the

physical properties of polymers [9]. Therefore, by selecting the appropriate nanofillers, the dielectric characteristics of polymer composites can be efficiently regulated [10].

As stated in the findings, embedding  $\text{TiO}_2$  nanoparticles within PVA/CN-Li polymer matrix and doping PVA with graphene oxide promotes electrical conductivity while giving enhanced optical, mechanical, and dielectric properties [11, 12]. According to the literature, pure polymer loaded with nanoparticles offers unique characteristics with diverse uses. When metal oxide nanoparticles are introduced to pure polymer, their characteristics improve dramatically. These compounds are exploited in industry for a variety of purposes, including battery electrodes, display systems, smart windows, lubricants, catalysts, and sensors [13–16]. In distinction, an n-type molybdenum trioxide ( $\text{MoO}_3$ ) semiconductor with a band gap of 3.15 eV is advantageous for a wide range of applications including electro and photochromism, sensors and catalysis, transistors, and portable battery electrodes [17, 18]. Wang et al. [19] studied the dielectric properties of barium titanate-molybdenum composite, prepared using solid state reaction in argon. The prepared composites showed superior dielectric properties and high dielectric constant. The incorporation of molybdenum ions in lead niobium germanosilicate glasses improved the dielectric properties. The distance between the Mo ions decreased with  $\text{MoO}_3$  concentrations and this reduction increased the chances of electron hopping, subsequently improving the ac conductivity and lowering the activation energy for conduction [20]. Malana et al. [21] also synthesized Molybdenum doped strontium calcium hexagonal ferrites using the sol-gel combustion method, and studied the structural, magnetic and dielectric properties. The dielectric parameters exhibited relaxation behavior in higher frequency region and showed an increasing trend with the molybdenum contents.

In this study, the biopolymer PVA composite containing variable quantities of  $\text{MoO}_3$  nanoparticles is synthesized by facile calcination treatment. XRD, FTIR, SEM, and impedance analyzer are used to investigate the microstructural, functional, morphological, electrical, and dielectric, characteristics. It is observed that the incorporation of 5 wt%  $\text{MoO}_3$  into PVA matrix achieved significantly high dielectric constant, suggesting its final application as a

separator/ionic transport media in high-performance energy storage devices.

## 2 Experimental section

### 2.1 Materials and methods

Pristine Molybdenum (III) oxide powder (99.5%, Sigma-Aldrich) was used as source material. Polyvinyl alcohol (PVA) of molecular weight 78,000 g/mol was purchased from Merck Schuchart, Germany. Ultra-pure Milli-Q water was used as a solvent throughout the study.

### 2.2 Preparation of MoO<sub>3</sub> rods

MoO<sub>3</sub> rods were synthesized from commercial Pristine MoO<sub>3</sub> powder by using facile calcination treatment and green way. About 2 g of MoO<sub>3</sub> was stirred continuously using a magnetic stirrer at 800 rpm for 15 min in 80 mL of deionized (DI) water. The solution was then poured into a 100 ml glass beaker and sonicated for an hour. After sonication, the solution was cleaned, sieved, and dried, in a hot air oven for 5 h at 150 °C. Thereafter the MoO<sub>3</sub> nanoparticles were collected.

### 2.3 Synthesis of PVA composites

The PVA composites containing MoO<sub>3</sub> were synthesized by solution casting. For this, about 2 g of PVA was dissolved in 20 ml distilled water by magnetic stirring (400 rpm) for 5 h at 70 °C. Bath sonication was used to disperse MoO<sub>3</sub> in precise weight fractions (1, 3, and 5 wt%) in the same solvent combination (5 ml) for 1 h before mixing with the PVA dispersions. To ensure optimal dispersion, the entire mixture was magnetically agitated overnight. The well-dispersed solution was then casted onto glass petri dish to form thin PVA and PVA/MoO<sub>3</sub> composite films.

The obtained films were dried at 80 °C for a few hours to completely remove any residual solvent in a hot air oven. Schematic representation of the composite film fabrication is shown in Fig. 1.

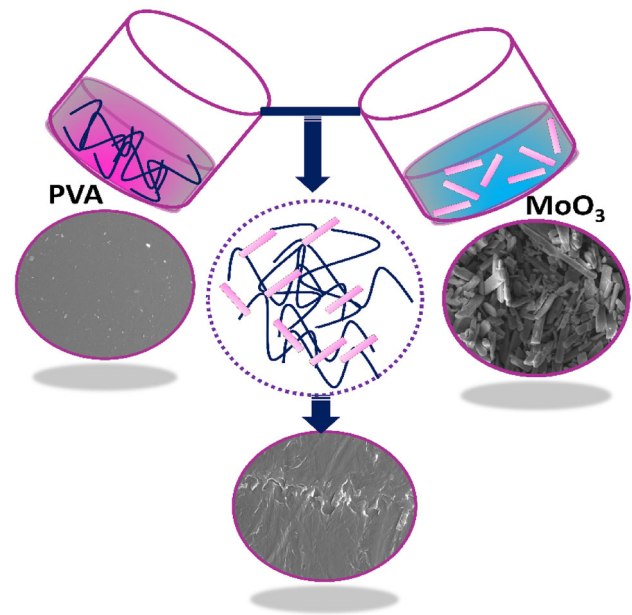


**Fig. 1** Schematic diagram for the synthesis process of PVA/MoO<sub>3</sub> polymer composite materials

### 2.4 Characterization techniques of PVA composites

Bruker built an X-ray diffractometer with a 1.540 wavelength and detection angles ranging from 10° to 60° to validate the structure of the composite films. The structure coordination of polymer chains was determined using a Shimadzu IR Tracer 100 spectrometer in the 4000–400 cm<sup>-1</sup> wavenumber range. The surface morphology and elemental analyses of the as-developed PVA/MoO<sub>3</sub> composite films were evaluated using a scanning electron microscopy (SEM) (Model: ZEISS-EVO 18 Research, Japan) attached with energy dispersive X-ray spectrometer (EDAX). The mechanical properties of the samples were monitored by a universal testing machine (Lloyd 1 KN LF plus, AMETEK, Inc., Bognor Regis, UK) at a speed rate of 5 mm min<sup>-1</sup>. The Hioki 3532-50 LCR Hi-tester serves to assess the impedance of composite films by applying potential at distinct frequencies (42 Hz to 1 MHz). In the LCR Hi-tester analysis, the resultant polymer composite is sandwiched between two silver electrodes. For the observed complex impedance, the overall resistances of the material are estimated using Z-view fitting software.

### 3 Result and discussion

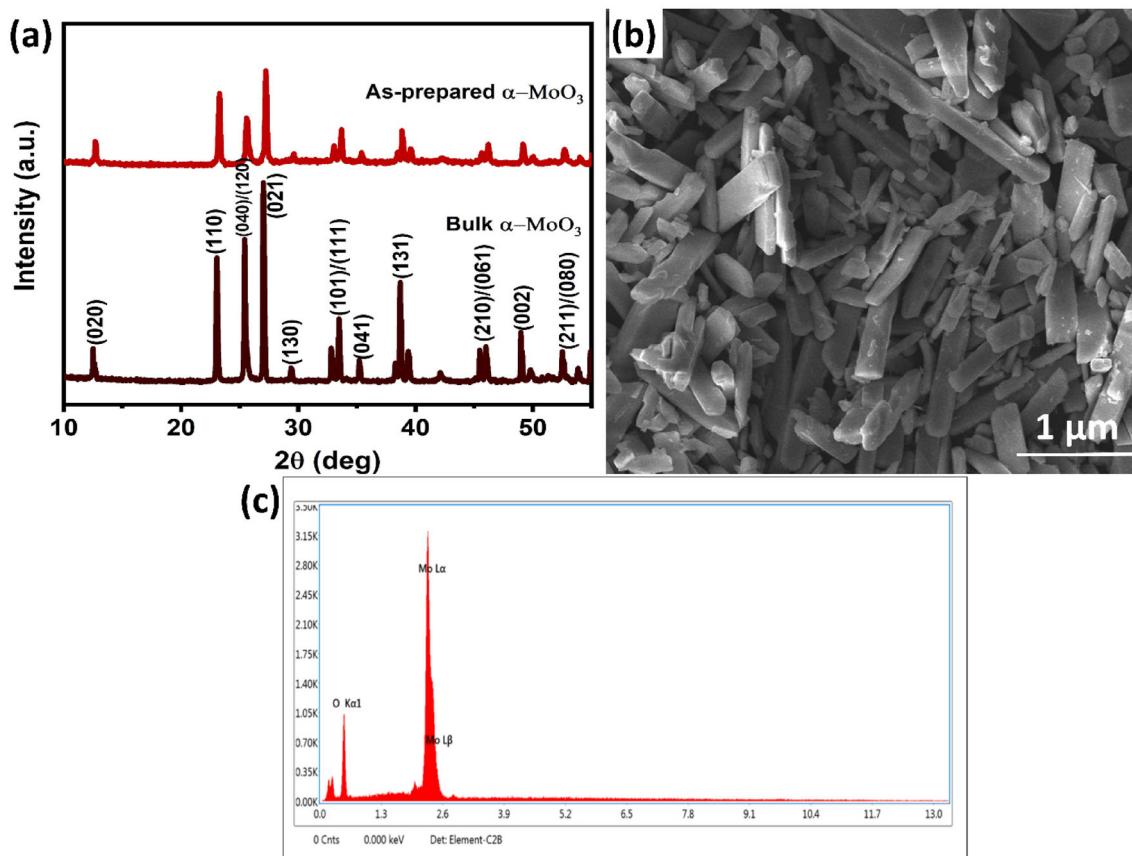
#### 3.1 Structural and morphological properties of the molybdenum oxide nanoparticles

Figure 2 displays the microstructures and crystallinity of as-prepared  $\text{MoO}_3$  nanostructures as evaluated by the SEM and X-ray diffraction (XRD) studies. The  $\text{MoO}_3$  sample (Fig. 1a) has diffraction peaks at  $12.93^\circ$ ,  $23.51^\circ$ ,  $26^\circ$ ,  $27.51^\circ$ ,  $29.66^\circ$ ,  $33.83^\circ$ ,  $35.68^\circ$ ,  $39.20^\circ$ ,  $46.47^\circ$ ,  $49.39^\circ$ ,  $52.75^\circ$ ,  $55.37^\circ$ ,  $57.65^\circ$ ,  $58.98^\circ$ ,  $64.62^\circ$ , and  $67.75^\circ$ . All these diffraction peaks can be attributed to orthorhombic  $\text{MoO}_3$  phase, which is consistent with standard JCPDS pattern (JCPDS #35-0609). The higher intensities of the (110), (040)/(120), and (021) diffraction peaks indicate that these nanostructures grew in a highly anisotropic manner. Furthermore, identical diffraction patterns are seen for the original material and the detected nanorods results same crystallinity with the reduced intensity and widening of the peaks after grinding is consistent

with smaller lateral dimensions [22]. It corresponded to JCPDS Card No. 05-0508 ( $\text{MoO}_3$ ) orthorhombic crystal structure. The morphology and composition of as-prepared  $\text{MoO}_3$  nanostructures were investigated using SEM and EDX. As shown in Fig. 2b, the  $\text{MoO}_3$  nanostructures were shown rod shaped dimension with an average diameter of 0.2 to 0.5  $\mu\text{m}$  and length of 1.5 to 3  $\mu\text{m}$ . The elemental analysis in Fig. 2c illustrates the presence of Mo and O only which confirms the successful formation of  $\text{MoO}_3$  structure.

#### 3.2 Structural and morphological properties of the PVA/molybdenum oxide composite films

Importantly, this work demonstrates green synthesis of  $\text{MoO}_3$  using water as a solvent. The bulk  $\text{MoO}_3$  possesses a tuneable layered structure. Water molecules have an affinity to intercalate into the  $\text{MoO}_3$  layers, which results in an expansion of the interlayer distances and thus weakness the bonds holding the



**Fig. 2** a Powder XRD patterns for bulk and  $\text{MoO}_3$  rods. b SEM image and c EDX spectrum of  $\text{MoO}_3$  rods

MoO<sub>3</sub> layers together. Consequently, the reflux of bulk MoO<sub>3</sub> in water at an elevated temperature can lead to its exfoliation into rods. The XRD spectra of PVA/MoO<sub>3</sub> (1, 3, and 5%) composites films are shown in Fig. 3. At a high concentration of 5 wt% MoO<sub>3</sub>, additional peaks at angles 12.44° (020), 25.4° (040), and 38.9° (060) are developed, confirming the MoO<sub>3</sub> existence in the final product [23–25]. The incorporation of MoO<sub>3</sub> filler improves the crystallinity of the PVA polymer [26]. For a polymer to be dielectric, crystallinity and planar orientation are crucial requirements. Here, the interfacial interactions are improved by the 5 wt% MoO<sub>3</sub> filler, which induces crystallinity in PVA and is thus expected to improve the dielectric properties. Various factors, including preparation methods and the presence of nanofillers within the polymer, are responsible for the PVA composite's higher crystallinity [27]. In Fig. 3b, the FTIR result reveals the functional assessment of MoO<sub>3</sub> filler added polymers in contrast to the pure sample. When the fraction of MoO<sub>3</sub> nanoparticles is increased, this peak reaches marginally to 3285 cm<sup>-1</sup>. The escalating hydrogen bonding is confirmed by the response of lower wave number peak change [28]. The intra/intermolecular H-bonding among the nanoparticles and the adjacent hydroxyl group of PVA were implicated for the recurrent changes in peak positions noticed upon filler addition. Secondly, the charge migration process among the PVA chains and nanoparticles is critical for the considerable alterations in peak position variations. The peaks found in the region of 2920–2927 cm<sup>-1</sup> correspond to asymmetric C–H

stretching vibrations. Besides that, the C = O stretching, C–H bending, and C–O elongation of PVA are likely responsible for the peak's appearance in the regions between 1640 and 1648, 1431 and 1436, and 1070 and 1095 cm<sup>-1</sup> [12, 29]. When the concentration of MoO<sub>3</sub> is increased, the intensity of the peaks changes, indicating that there is a substantial interplay between the pure polymer and MoO<sub>3</sub> [30].

SEM is a useful technique for studying the morphology of materials. As evident in the SEM images (Fig. 4), structural alterations occur in the samples as a result of MoO<sub>3</sub> interactions with pure PVA. A uniform and homogenous surface (Fig. 4a) confirms the miscibility of MoO<sub>3</sub> in PVA. When compared to the pure PVA, there is an influence of MoO<sub>3</sub> dispersions in the sample containing 1 wt% MoO<sub>3</sub> (Fig. 4b). We see considerable changes in morphological growth when the filler level is increased to 3 wt% (Fig. 4c), which could impact the strong interfacial interaction between filler and polymer matrix. At 5 wt% MoO<sub>3</sub>, the MoO<sub>3</sub> fillers are uniformly distributed throughout the polymer, as illustrated in Fig. 4d. Additionally, no surface defects or cracks were observed on the surface of the composite films. These findings imply that the composite films are flexible. The well dispersed and uniform particle nature improves the dielectric properties of the polymer matrix.

### 3.3 Mechanical properties

The tensile tests on the pure PVA and PVA/MoO<sub>3</sub> composite films were carried out in order to evaluate

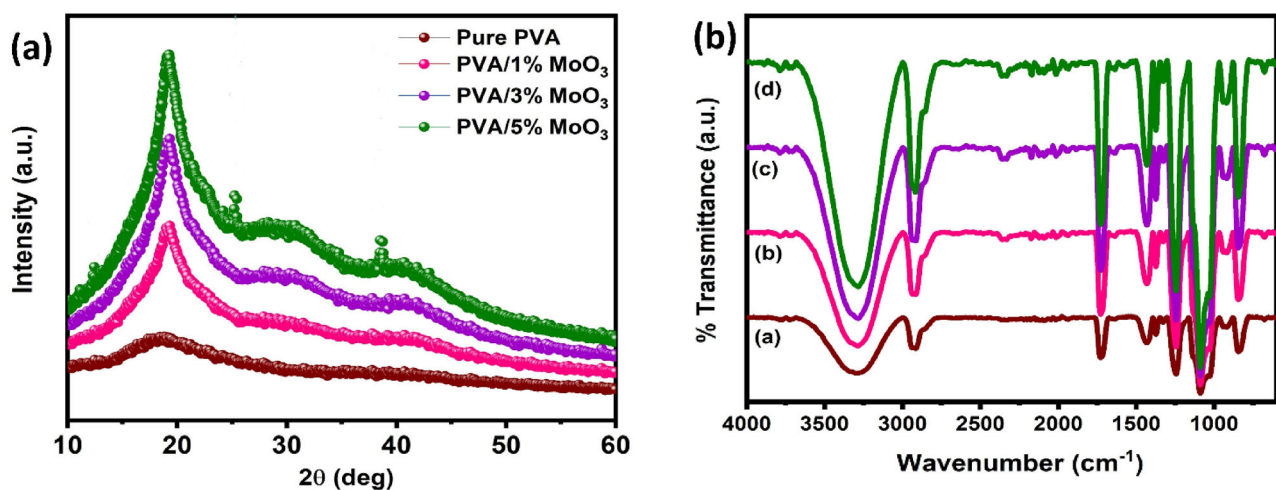
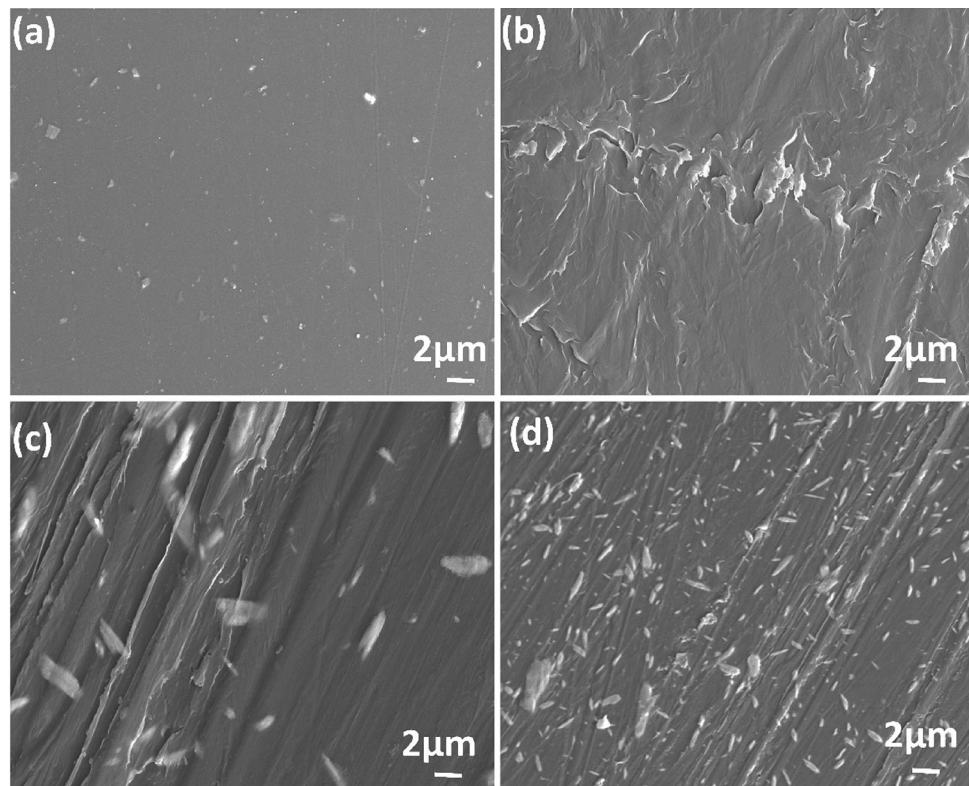


**Fig. 3** a XRD and b FTIR spectra of pure PVA and at various wt% of MoO<sub>3</sub>

**Fig. 4** SEM images of PVA pure doped with (a) 0.0 wt%, (b) 1 wt%, (c) 3 wt% and (d) 5 wt% of MoO<sub>3</sub> nanoparticles



the influence of MoO<sub>3</sub> fillers on the mechanical properties of PVA and its composites. It was observed that the mechanical properties of the composite films can be improved significantly, due to the strong adhesion between MoO<sub>3</sub> filler and PVA matrix resulting from the hydrogen bonding interactions. The mechanical properties such as tensile strength, Young's modulus and percent elongation at break evaluated from the tensile tests are provided in Table 1. From the Table 1, the tensile properties of the PVA/MoO<sub>3</sub> composite films increased compared to the pure PVA. The mechanical reinforcement with MoO<sub>3</sub> was believed to be due to an effective interfacial load transfer resulting from the enhanced interfacial adhesion between the polymer matrixes and the fillers [26].

### 3.4 Electrical properties of the composite films

In order to construct composite materials with superior dielectric properties, the effects of varying MoO<sub>3</sub> volume fractions in the PVA/MoO<sub>3</sub> particles on the electrical properties were investigated. Figure 5a depicts a Nyquist curve derived from EIS findings in the 1 Hz to 100 kHz frequency range. Figure 5b depicts the differences in ac conductivity between composites with MoO<sub>3</sub> doping and a pure sample. The ac conductivity increases with the concentration of MoO<sub>3</sub> nanoparticles until it reaches 5% by weight. In all films, conductivity increases with frequency (Table 2). The bonds are designed to switch at higher frequencies, resulting in a dielectric transition with vulnerable trustworthy polar functional groups, which causes physiological

**Table 1** Mechanical properties of the composites

Sample	Tensile strength (MPa)	Young's modulus (MPa)	Elongation at break (%)
PVA	18.21 ± 1.90	65.30 ± 9.21	10.21 ± 0.65
PVA/1% MoO <sub>3</sub>	25.31 ± 2.0	74.32 ± 6.00	9.23 ± 1.10
PVA/3% MoO <sub>3</sub>	36.21 ± 1.8	88.24 ± 7.21	8.42 ± 1.22
PVA/ 5% MoO <sub>3</sub>	40.21 ± 2.1	92.54 ± 9.01	7.21 ± 0.98

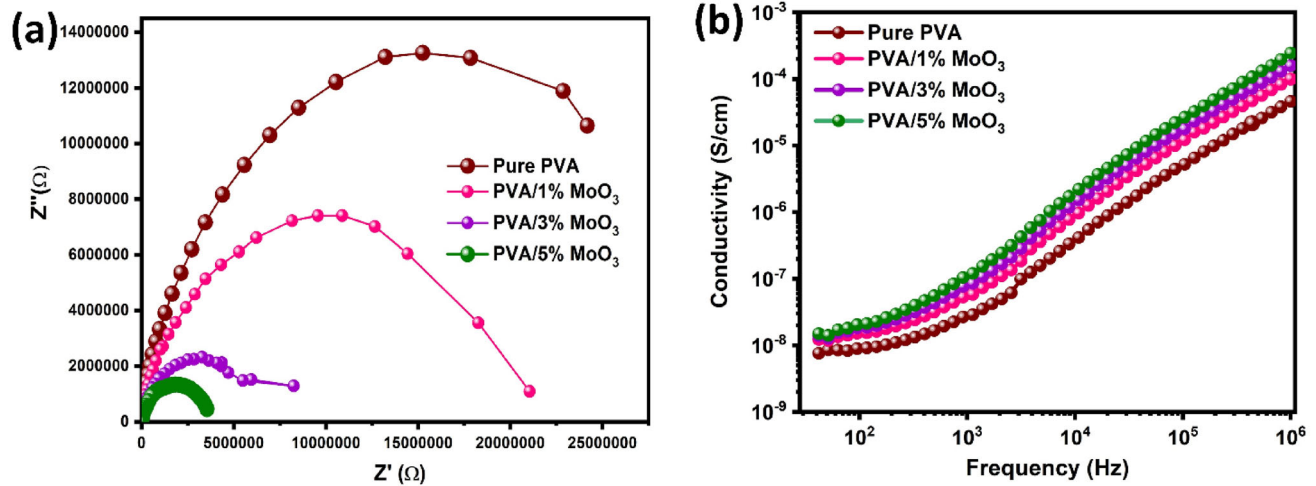


**Fig. 5** a and b Variation of ac conductivity with frequency for pure and different PVA (1, 3 and 5%) added molybdenum oxide composite films

**Table 2** Electrical conductivity ( $\sigma_{dc}$ ) and relaxation time for PVA/MoO<sub>3</sub> composite films

Sample	$\sigma_{dc}$ (s/cm)	Relaxation time (in sec)
PVA/1wt% MoO <sub>3</sub>	$7.314 \times 10^{-9}$	$1.2 \times 10^{-3}$
PVA/3wt% MoO <sub>3</sub>	$1.416 \times 10^{-8}$	$1.4 \times 10^{-3}$
PVA/5wt% MoO <sub>3</sub>	$2.8 \times 10^{-8}$	$2.6 \times 10^{-4}$

adaptations within the polymer structure via the formation of charge transfer complexes, implying increased electrical conductivity of the films [31, 32].

The complex permittivity,  $\epsilon^*$  comprises real and imaginary parts and provides detail information about the polarization mechanism [33] and it is given by:  $\epsilon^* = \epsilon' - j\epsilon''$

The real part ( $\epsilon'$ ) and imaginary part ( $\epsilon''$ ) of complex permittivity are given as

$$\epsilon' = \frac{-Z''}{\omega C_0(Z'^2 + Z''^2)} \text{ and } \epsilon'' = \frac{Z'}{\omega C_0(Z'^2 + Z''^2)}$$

Here,  $Z'$  is real part, and  $Z''$  is imaginary part of impedance,  $f$  is the applied frequency ( $\omega = 2\pi f$ ),  $C_0 = (\epsilon_0 A/t)$ ,  $A$  is the area and  $t$  is the thickness of the sample.

The frequency dependent values of the dielectric constant' and dielectric loss' of the PVA/MoO<sub>3</sub> composites samples are shown in Fig. 6. A dielectric material's electrical energy strong ability (i.e., the strength of dielectric polarization) under the influence of a time-varying electric field is measured by

the dielectric constant value, whereas the dielectric loss value represents the electrical energy loss per cycle due to the Joule heating effect [11]. The difference in the dielectric constant ( $\epsilon'$ ) with respect to log ( $f$ ) shows that the dielectric constant rises at lower frequencies and falls at higher frequencies. This increased dielectric constant is due to Maxwell-Wagner polarization, which is primarily produced by conductor-insulator interactions. Furthermore, this interfacial polarization is caused by the accumulation of space charge polarization at the interfaces.

Space charges acquire ample time to adapt to an applied electric field in the low-frequency region; but, in the higher frequency range, changes towards an electric field eventuate rapidly for space charges to adjust, and the polarization consequence could not exist. In the sample where percolation occurs, PVA with 5% MoO<sub>3</sub> doping possesses greatest possible dielectric constant. Over this percolation threshold, the dielectric constant tends to decrease [34–37]. As demonstrated in Fig. 6b, the dielectric loss ( $\epsilon''$ ) reduces as the frequency increases. Higher frequencies hinder the ability for space charges that respond towards the applied field, therefore charge accumulation due to polarization reduces, and hence dielectric loss decreases [38]. The dielectric loss factor is a standard definition of power outage in a dielectric medium ( $\tan \delta$ ). The frequency evolution of the dielectric loss factor for all films is shown in Fig. 6c. Tangent loss decreases as frequency increases, as seen by the graph. Dielectric loss can similarly be

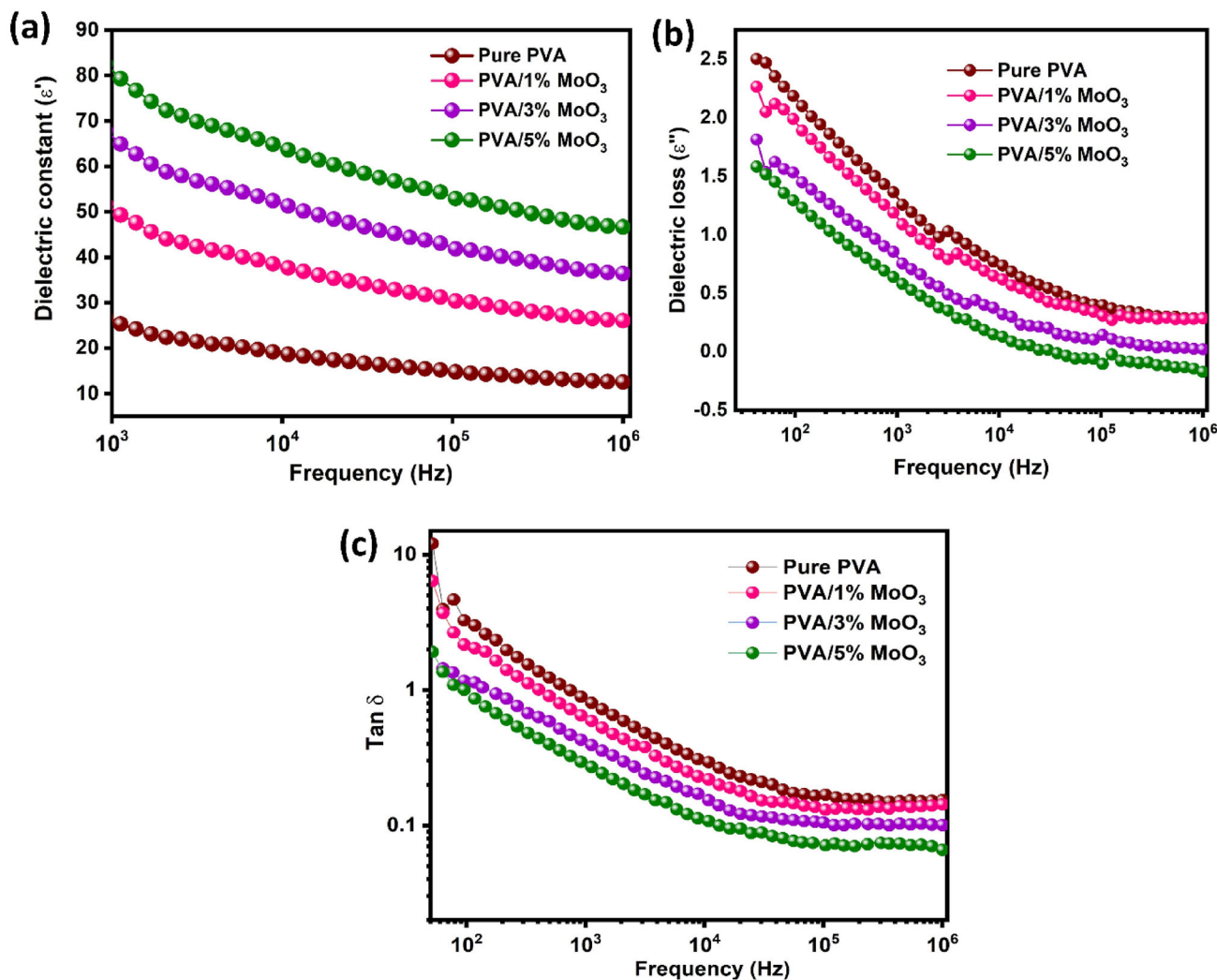


**Fig. 6** a Variation of dielectric constant, b Variation of dielectric loss ( $\epsilon''$ ) and c Variation of dielectric loss factor with frequency for pure different PVA (1, 3 and 5%) added molybdenum oxide composites films

expressed in terms of the loss tangent ( $\tan \delta$ ), and is denoted as

$$\tan \delta = \frac{\epsilon''}{\epsilon'}$$

Where  $\epsilon'$  is dielectric constant and  $\epsilon''$  is dielectric loss [39]. It is observed that the  $\tan$  values of these polymer composite materials are significantly small, indicating that they are suitable as a potential candidate for the fabrication of electronic devices. The maximum peak corresponding frequency of  $\tan \delta$  spectra is used to evaluate the relaxation time  $\tau =$

$\left(\frac{1}{2\pi f_{max}}\right)$ , (Where  $f_{max}$  is the frequency corresponding to peak maxima in the  $\tan \delta$  vs.  $f$  plot) and is summarized in Table 1. The lowest relaxation time is

observed for the 5%  $\text{MoO}_3$  filler. This result demonstrates that the filler content of these polymer composite materials significantly influences the electrostatic interactions between filler and polymer.

Analyzing the modulus ( $M^*$ ) provides more insight into the loss tangent and dielectric permittivity analysis. The ability to separate the polarization effect from the bulk relaxation phenomenon in the polymer electrolyte is one advantage of modulus analysis [40]. Complex electric modulus ( $M^*$ ) and complex permittivity ( $\epsilon^*$ ) are connected by the following equations.

$$M^* = M + jM'' = \frac{\epsilon}{(\epsilon)^2 + \epsilon''^2} + j \frac{\epsilon''}{(\epsilon)^2 + \epsilon''^2}$$



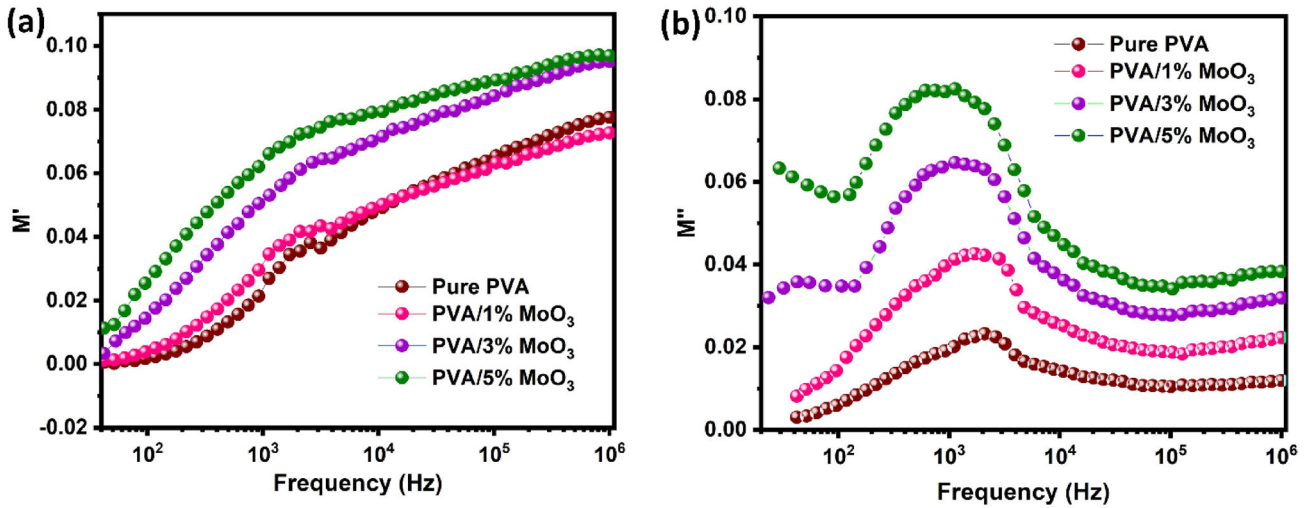


**Fig. 7** Frequency dependent real part  $M'$  and loss part  $M''$  for pure different PVA (1, 3 and 5%) added molybdenum oxide composites films

**Fig. 8** Schematic representation of uniform dispersion of filler in the polymer matrix

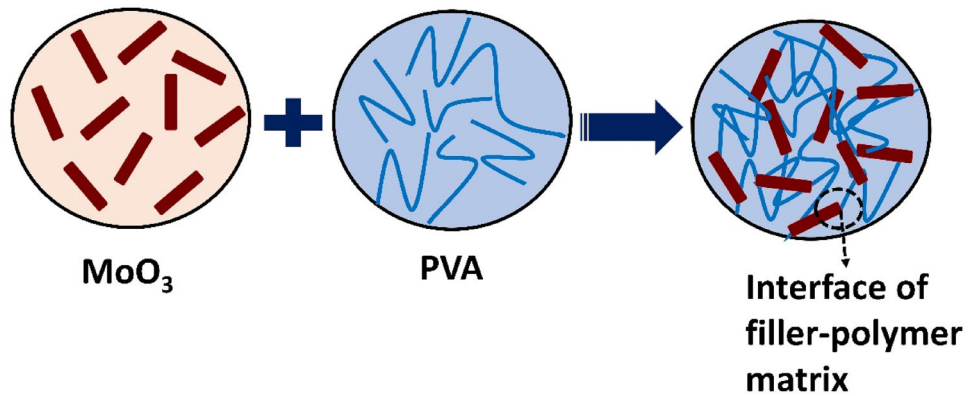


**Table 3** Comparison of dielectric constant, dielectric loss of the PVA composite films containing  $\text{MoO}_3$  particles

Fillers	Polymer Matrix	Dielectric constant	References
BT microparticles	Resin	32	[44]
BT nanoparticles/BN nanosheet	PVDF-HFP	11.7	[45]
BT@ $\text{Al}_2\text{O}_3$ nanoparticles	PVDF	17.5	[46]
Sphere-like $\text{TiO}_2$ nanowire	PVDF-HFP	11.9	[47]
$\text{CaCu}_3\text{Ti}_4\text{O}_{12}$ @ $\text{TiO}_2$	Polyimide	5.85	[48]
$\text{MoO}_3$	Polyvinyl alcohol	80	This work

Whereas  $M'$  is the real dielectric modulus and  $M''$  is an imaginary component. Figure 7a, b depicts how the real and imaginary parts of the modulus. Figure 7a shows a dispersion region for the polymer composite films, and the long tail is located in a low-frequency region. The  $M'$  value increases rapidly at high frequencies, and the high-frequency window contains the peak for the 5%  $\text{MoO}_3$  [41]. The variation

of  $M''$  with frequency is reported to have the same characteristic. The widening in the peak of the modulus plots ( $M'$  &  $M''$ ) at higher frequency side indicates the dominance of non-debye type relaxation behavior in such systems [42].

The  $M'$  values are seen to rise irregularly with increase in frequency, eventually hitting a constant—current near 1 MHz. The  $M''$  spectrum of the 3 wt%  $\text{MoO}_3$  doped PVA composite film revealed distinct

relaxation signals in the fairly low and intermediate frequency ranges, but merely the relaxation spike in the midway frequency range was detected for the remaining wt% MoO<sub>3</sub> and pure PVA samples (Fig. 7b). The low-frequency peak is experienced by the MWS relaxation process, that has been detected in previous polymeric composites [43], but the intermediate frequency zone peak is formed by the PVA chain segmental movements (-relaxation) of the polymers composite materials studied.

Properties of polymer composites are influenced by three main factors, including filler surface properties, nano reinforcing properties, and interfacial interactions between the two. The properties of a polymeric composite also heavily depend on the dispersion and distribution of fillers in the continuous matrix phase for a specific nano reinforcement phase and matrix polymer (Fig. 8).

Table 3 compares the dielectric properties of some polymer/filler composite films reported previously. One can find that the PVA/MoO<sub>3</sub> composite films prepared by green method in this work shows good dielectric properties (i.e., high dielectric constant and low dielectric loss). The high dielectric constant of the composite films is due to the uniform distribution of MoO<sub>3</sub> fillers in the PVA matrix.

## 4 Conclusion

In summary, we have successfully prepared PVA/MoO<sub>3</sub> composite films by facile and green method. The structural characterization of the samples explored by XRD and FTIR studies. With different wt% ratios of MoO<sub>3</sub> added to a PVA polymer matrix, dielectric relaxation and conductivity studies have been investigated. The polymer composite films' dielectric constant increases as filler MoO<sub>3</sub> content increases, reaching its highest level at 5 wt% loading. High conductivity is achieved by dopant ions with the highest dielectric constant. Analysis of the loss tangent spectra reveals a decrease in the relaxation time. It has been found that the conductivity of polymer composite films increases with MoO<sub>3</sub> concentration and reaches its maximum value ( $\sim 10^{-8}$  S/cm) for the 5 wt% of MoO<sub>3</sub> content. Additionally, modulus study supported the above conclusions. The 5 wt% MoO<sub>3</sub>/polymer composite films showed the lowest value of relaxation time. The prepared polymer composite films may be used as

separator/ionic transport media for high-performance energy devices due to their high dielectric constant, conductivity, and low relaxation time.

## Author contributions

All authors contributed significantly to the study conception and design. Data generation, collection and analysis were performed by (KP). The first draft of the manuscript was written by (KP), (VS), and (AB), and the other authors (PSV) and (DP) revised the article with timely suggestions for improvement. All authors read and approved the final manuscript.

## Funding

Open Access funding provided by the Qatar National Library. The authors have not disclosed any funding.

## Data availability

No data were used.

## Declarations

**Conflict of interest** The authors have no relevant financial or non-financial interests to disclose.

**Open Access** This article is licensed under a Creative Commons Attribution 4.0 International License, which permits use, sharing, adaptation, distribution and reproduction in any medium or format, as long as you give appropriate credit to the original author(s) and the source, provide a link to the Creative Commons licence, and indicate if changes were made. The images or other third party material in this article are included in the article's Creative Commons licence, unless indicated otherwise in a credit line to the material. If material is not included in the article's Creative Commons licence and your intended use is not permitted by statutory regulation or exceeds the permitted use, you will need to obtain permission directly from the copyright holder. To view a copy of this licence, visit <http://creativecommons.org/licenses/by/4.0/>.

## References

1. X. Zhang et al., Ultrahigh energy density of polymer nanocomposites containing BaTiO<sub>3</sub>@ TiO<sub>2</sub> nanofibers by atomic-scale interface engineering. *Adv. Mater.* **27**(5), 819–824 (2015)
2. D. Ponnamma, M.A.A. Al-Maadeed, 3D architectures of titania nanotubes and graphene with efficient nanosynergy for supercapacitors. *Mater. Design.* **117**, 203–212 (2017)
3. K. Digvijay Satapathy et al., High-quality factor poly (vinylidene fluoride) based novel nanocomposites filled with graphene nanoplatelets and vanadium pentoxide for high-Q capacitor applications. *Adv. Mater. Lett.* **8**(3), 288–294 (2017)
4. Q.G. Chi, J.F. Dong, C.H. Zhang, C.P. Wong, X. Wang, Q.Q. Lei, Nano iron oxide-deposited calcium copper titanate/polyimide hybrid films induced by an external magnetic field: toward a high dielectric constant and suppressed loss. *J. Mater. Chem. C* **4**(35), 8179–8188 (2016)
5. B. Ben Doudou, A. Vivet, J. Chen, A. Laachachi, T. Falher, C. Poilâne, Hybrid carbon nanotube—silica/polyvinyl alcohol nanocomposites films: preparation and characterisation. *J. Polym. Res.* **21**(4), 1–9 (2014)
6. R. Kochi, V. Crasta, R. Kumar, G. Shetty, 2019 Study of structural, optical and photoluminescence properties of ZnO doped PVA/PVP nanocomposite, In: *AIP Conference Proceedings*, AIP Publishing LLC
7. B.M. Baraker, B. Lobo, Experimental study of PVA-PVP blend films doped with cadmium chloride monohydrate, 2016
8. B. Pradhan, K. Setyowati, H. Liu, D.H. Waldeck, J. Chen, Carbon nanotube—polymer nanocomposite infrared sensor. *Nano Lett.* **8**(4), 1142–1146 (2008)
9. X. Yang, L. Li, S. Shang, X. Tao, Synthesis and characterization of layer-aligned poly (vinyl alcohol)/graphene nanocomposites. *Polymer* **51**(15), 3431–3435 (2010)
10. F. Liu et al., Poly (methyl methacrylate)/boron nitride nanocomposites with enhanced energy density as high temperature dielectrics. *Compos. Sci. Technol.* **142**, 139–144 (2017)
11. S.G. Rathod et al., Pressure sensitive dielectric properties of TiO<sub>2</sub> doped PVA/CN-Li nanocomposite. *J. Polym. Res.* **22**(2), 1–14 (2015)
12. S.G. Rathod, R. Bhajantri, V. Ravindrachary, J. Naik, D.M. Kumar, High mechanical and pressure sensitive dielectric properties of graphene oxide doped PVA nanocomposites. *RSC Adv.* **6**(81), 77977–77986 (2016)
13. M.M. Alsaif et al., Tunable plasmon resonances in two-dimensional molybdenum oxide nanoflakes. *Adv. Mater.* **26**(23), 3931–3937 (2014)
14. D. Chen et al., Single-crystalline MoO<sub>3</sub> nanoplates: topochemical synthesis and enhanced ethanol-sensing performance. *J. Mater. Chem.* **21**(25), 9332–9342 (2011)
15. S. Balendhran et al., Field effect biosensing platform based on 2D  $\alpha$ -MoO<sub>3</sub>. *ACS Nano* **7**(11), 9753–9760 (2013)
16. Y.-J. Chen et al., “Porous iron molybdate nanorods: in situ diffusion synthesis and low-temperature H<sub>2</sub>S gas sensing”. *ACS Appl. Mater. Interfaces* **5**(8), 3267–3274 (2013)
17. Y. Wang et al., 2014 Liquid-phase growth of platinum nanoparticles on molybdenum trioxide nanosheets: an enhanced catalyst with intrinsic peroxidase-like catalytic activity. *Nanoscale*, 6.21:12340–12344,
18. P. Wongkrua, T. Thongtem, S. Thongtem, “J. Nanomater,” ed, 2013
19. B. Wang, Y.-P. Pu, N. Xu, H.-D. Wu, K. Chen, “Dielectric properties of barium titanate—molybdenum composite,”. *Ceram. Int* **38**, S37–S40 (2012)
20. T. Narendrudu, S. Suresh, A.S. Kumar, M.S. Rao, P.S. Rao, D.K. Rao, Spectroscopic and dielectric investigations on the role of molybdenum ions in lead niobium germanosilicate glasses. *J. Non-cryst. Solids* **442**, 44–55 (2016)
21. M.A. Malana, R.B. Qureshi, M.N. Ashiq, M.F. Ehsan, “Synthesis, structural, magnetic and dielectric characterizations of molybdenum doped calcium strontium M-type hexaferrites”. *Ceram. Int* **42**(2), 2686–2692 (2016)
22. Z. Wang, S. Madhavi, X.W. Lou, Ultralong  $\alpha$ -MoO<sub>3</sub> nanobelts: synthesis and effect of binder choice on their lithium storage properties. *J. Phys. Chem. C* **116**(23), 12508–12513 (2012)
23. X.W. Lou, H.C. Zeng, Hydrothermal synthesis of  $\alpha$ -MoO<sub>3</sub> nanorods via acidification of ammonium heptamolybdate tetrahydrate. *Chem. Mater* **14**(11), 4781–4789 (2002)
24. L. Noerochim, J.-Z. Wang, D. Wexler, Z. Chao, H.-K. Liu, Rapid synthesis of free-standing MoO<sub>3</sub>/Graphene films by the microwave hydrothermal method as cathode for bendable lithium batteries. *J. Power Sources* **228**, 198–205 (2013)
25. M.A. Ibrahim et al., High quantity and quality few-layers transition metal disulfide nanosheets from wet-milling exfoliation. *RSC Adv.* **3**(32), 13193–13202 (2013)
26. S.K. Pasha, K. Deshmukh, M.B. Ahamed, K. Chidambaram, M. Mohanapriya, N.A.N. Raj, Investigation of microstructure, morphology, mechanical, and dielectric properties of PVA/PbO nanocomposites. *Adv. Polym. Technol.* **36**(3), 352–361 (2017)
27. H. Parangusan, D. Ponnamma, M.A.A. AlMaadeed, Investigation on the effect of  $\gamma$ -irradiation on the dielectric and piezoelectric properties of stretchable PVDF/Fe–ZnO nanocomposites for self-powering devices. *Soft Matter.* **14**(43), 8803–8813 (2018)

28. S. Srivastava, S. Kumar, V. Singh, M. Singh, Y. Vijay, Synthesis and characterization of TiO<sub>2</sub> doped polyaniline composites for hydrogen gas sensing. *Int. J. Hydrog. Energy* **36**(10), 6343–6355 (2011)
29. Z.N. Kayani, A. Shahzadi, S. Riaz, S. Naseem, Preparation and characterization of dip coated cobalt oxide thin films. *Mater. Res. Innov.* **23**(5), 253–259 (2019)
30. H. Zidan, N. El-Ghamaz, A. Abdelghany, A. Lotfy, Structural and electrical properties of PVA/PVP blend doped with methylene blue dye. *Int. J. Electrochem. Sci.* **11**, 9041–9056 (2016)
31. E. Abdelrazek, I. Elashmawi, A. El-Khodary, A. Yassin, Structural, optical, thermal and electrical studies on PVA/PVP blends filled with lithium bromide. *Curr. Appl. Phys.* **10**(2), 607–613 (2010)
32. H. Woo, S.R. Majid, A.K. Arof, Dielectric properties and morphology of polymer electrolyte based on poly ( $\epsilon$ -caprolactone) and ammonium thiocyanate. *Mater. Chem. Phys.* **134**, 2–3 (2012)
33. F. Kremer, A. Schönhal, 2002 Broadband Dielectric Spectroscop. Springer Science & Business Media, NY
34. K. Rajesh, V. Crasta, N. Rithin Kumar, G. Shetty, P. Rekha, Structural, optical, mechanical and dielectric properties of titanium dioxide doped PVA/PVP nanocomposite. *J. Polym. Res.* **26**(4), 1–10 (2019)
35. N.R. Kumar, V. Crasta, B. Praveen, Dielectric and electric conductivity studies of PVA (Mowiol 10–98) doped with MWCNTs and WO<sub>3</sub> nanocomposites films. *Mater. Res. Express* **3**(5), 055012 (2016)
36. M. Khan, A.N. Khan, A. Saboor, I.H. Gul, Investigating mechanical, dielectric, and electromagnetic interference shielding properties of polymer blends and three component hybrid composites based on polyvinyl alcohol, polyaniline, and few layer graphene. *Polym. Compos.* **39**(10), 3686–3695 (2018)
37. S. Ravati, B.D. Favis, 2010 Low percolation threshold conductive device derived from a five-component polymer blend. *Polymer*, 51.16:3669–3684
38. M. Buraidah, L. Teo, S. Majid, A. Arof, Ionic conductivity by correlated barrier hopping in NH<sub>4</sub>I doped chitosan solid electrolyte. *Phys. B: Condens. Matter.* **404**, 8–11 (2009)
39. V. Duraikkan, A.B. Sultan, N. Nallaperumal, A. Shunmuganarayanan, 2018 Structural, thermal and electrical properties of polyvinyl alcohol/poly (vinyl pyrrolidone)–sodium nitrate solid polymer blend electrolyte. *Ionics*, 24.1:139–151
40. A. Arya, A.L. Sharma, Temperature and salt-dependent dielectric properties of blend solid polymer electrolyte complexed with LiBOB. *Macromol. Res.* **27**(4), 334–345 (2019)
41. S.B. Aziz, S.M. Mamand, The study of dielectric properties and conductivity relaxation of ion conducting chitosan: NaTf based solid electrolyte. *Int. J. Electrochem. Sci.* **13**, 10274–10288 (2018)
42. C. Mao, Y. Zhu, W. Jiang, Design of electrical conductive composites: tuning the morphology to improve the electrical properties of graphene filled immiscible polymer blends. *ACS Appl. Mater. Interfaces* **4**(10), 5281–5286 (2012)
43. S. Mahendia, A. Tomar, S. Kumar, Nano-Ag doping induced changes in optical and electrical behaviour of PVA films. *Mater. Sci. Eng.: B* **176**(7), 530–534 (2011)
44. L. Gu et al., 2019 Effects of the particle size of BaTiO<sub>3</sub> fillers on fabrication and dielectric properties of BaTiO<sub>3</sub>/Polymer/Al films for capacitor energy-storage application. *Materials*, 12.3:439
45. Y. Xie, J. Wang, Y. Yu, W. Jiang, Z. Zhang, Enhancing breakdown strength and energy storage performance of PVDF-based nanocomposites by adding exfoliated boron nitride. *Appl. Surf. Sci.* **440**, 1150–1158 (2018)
46. D. He, Y. Wang, X. Chen, Y. Deng, Core-shell structured BaTiO<sub>3</sub>@ Al<sub>2</sub>O<sub>3</sub> nanoparticles in polymer composites for dielectric loss suppression and breakdown strength enhancement. *Compos. Part A: Appl. Sci. Manufac.* **93**, 137–143 (2017)
47. Q. Huang, H. Luo, C. Chen, K. Zhou, D. Zhang, Improved energy density and dielectric properties of P (VDF-HFP) composites with TiO<sub>2</sub> nanowire clusters. *J. Electroceram.* **40**, 65–71 (2018)
48. J. Wang, Y. Long, Y. Sun, X. Zhang, H. Yang, B. Lin, Fabrication and enhanced dielectric properties of polyimide matrix composites with core-shell structured CaCu<sub>3</sub> Ti<sub>4</sub> O<sub>12</sub>@ TiO<sub>2</sub> nanofibers. *J. Mater. Sci.: Mater. Electron.* **29**, 7842–7850 (2018)

**Publisher's Note** Springer Nature remains neutral with regard to jurisdictional claims in published maps and institutional affiliations.